




## Quantum-critical scale invariance in a transition metal alloy

Yasuyuki Nakajima<sup>1,2</sup><sup>✉</sup>, Tristin Metz<sup>2</sup>, Christopher Eckberg<sup>2</sup>, Kevin Kirshenbaum<sup>2</sup>, Alex Hughes<sup>2</sup>, Renxiong Wang<sup>2</sup>, Limin Wang<sup>2</sup>, Shanta R. Saha<sup>2</sup>, I-Lin Liu<sup>2,3,4</sup>, Nicholas P. Butch<sup>2,4</sup>, Daniel Campbell<sup>2</sup>, Yun Suk Eo<sup>2</sup>, David Graf<sup>5</sup><sup>5</sup>, Zhonghao Liu<sup>6,7</sup>, Sergey V. Borisenko<sup>6</sup>, Peter Y. Zavalij<sup>8</sup> & Johnpierre Paglione<sup>2,9</sup><sup>2,9</sup><sup>✉</sup>

Quantum-mechanical fluctuations between competing phases induce exotic collective excitations that exhibit anomalous behavior in transport and thermodynamic properties, and are often intimately linked to the appearance of unconventional Cooper pairing. High-temperature superconductivity, however, makes it difficult to assess the role of quantum-critical fluctuations in shaping anomalous finite-temperature physical properties. Here we report temperature-field scale invariance of non-Fermi liquid thermodynamic, transport, and Hall quantities in a non-superconducting iron-pnictide,  $\text{Ba}(\text{Fe}_{1/3}\text{Co}_{1/3}\text{Ni}_{1/3})_2\text{As}_2$ , indicative of quantum criticality at zero temperature and applied magnetic field. Beyond a linear-in-temperature resistivity, the hallmark signature of strong quasiparticle scattering, we find a scattering rate that obeys a universal scaling relation between temperature and applied magnetic fields down to the lowest energy scales. Together with the dominance of hole-like carriers close to the zero-temperature and zero-field limits, the scale invariance, isotropic field response, and lack of applied pressure sensitivity suggests a unique quantum critical system unhindered by a pairing instability.

<sup>1</sup> Department of Physics, University of Central Florida, Orlando, FL 32816, USA. <sup>2</sup> Maryland Quantum Materials Center, Department of Physics, University of Maryland, College Park, MD 20742, USA. <sup>3</sup> Chemical Physics Department, University of Maryland, College Park, MD 20742, USA. <sup>4</sup> NIST Center for Neutron Research, National Institute of Standards and Technology, Gaithersburg, MD 20899, USA. <sup>5</sup> National High Magnetic Field Laboratory, Florida State University, Tallahassee, FL 32310, USA. <sup>6</sup> IFW-Dresden, Helmholtzstraße 20, 01069 Dresden, Germany. <sup>7</sup> Shanghai Institute of Microsystem and Information Technology, Chinese Academy of Sciences, Shanghai 200050, China. <sup>8</sup> Department of Chemistry, University of Maryland, College Park, MD 20742, USA. <sup>9</sup> The Canadian Institute for Advanced Research, Toronto M5G 1Z8 ON, Canada. ✉email: [yasuyuki.nakajima@ucf.edu](mailto:yasuyuki.nakajima@ucf.edu); [paglione@umd.edu](mailto:paglione@umd.edu)

**N**on-Fermi liquid (NFL) behavior ubiquitously appears in iron-based high-temperature superconductors with a novel type of superconducting pairing symmetry driven by interband repulsion<sup>1, 2</sup>. The putative pairing mechanism is thought to be associated with the temperature-doping phase diagram, bearing striking resemblance to cuprate and heavy-fermion superconductors<sup>3, 4</sup>. In iron-based superconductors, the superconducting phase appears to be centered around the point of suppression of antiferromagnetic (AFM) and orthorhombic structural order<sup>1</sup>. Close to the boundary between AFM order and superconductivity, the exotic metallic regime emerges in the normal state. The “strange” metallic behavior seems to be universal in strongly correlated metals near a quantum critical point (QCP), characterized by linear-in- $T$  resistivity<sup>5–8</sup>. The universal transport behavior is known as Planckian dissipation, where the transport scattering rate is constrained by thermal energy,  $\hbar/\tau_p = k_B T$ , where  $\hbar$  is the reduced Planck constant and  $k_B$  is the Boltzmann constant. Lacking an intrinsic energy scale, the scale-invariant transport in strange metals is one of the unresolved phenomena in condensed matter physics, but its microscopic origin has yet to be fully understood. In iron-based superconductors, along with the AFM order, the presence of an electronic nematic phase above the structural transition complicates the understanding of the superconductivity and NFL behavior<sup>9–12</sup>. Moreover, the robust superconducting phase prohibits investigations of zero-temperature limit normal state physical properties associated with the quantum critical (QC) instability due to the extremely high upper critical fields.

While AFM spin fluctuations are widely believed to provide the pairing glue in the iron pnictides, other magnetic interactions are prevalent in closely related materials, such as the cobalt-based oxypnictides  $\text{LaCoOX}$  ( $X = \text{P}, \text{As}$ )<sup>13</sup>, which exhibit ferromagnetic (FM) orders, and Co-based intermetallic arsenides with coexisting FM and AFM spin correlations<sup>14–16</sup>. For instance, a strongly enhanced Wilson ratio  $R_W$  of  $\sim 7\text{--}10$  at 2 K (ref. 17) and violation of the Korringa law<sup>14–16</sup> suggest proximity to a FM instability in  $\text{BaCo}_2\text{As}_2$ .  $\text{BaNi}_2\text{As}_2$ , on the other hand, seems to be devoid of magnetic order<sup>18</sup> and rather hosts other ordering instabilities in both structure and charge<sup>19</sup>. Confirmed by extensive study, Fe, Co, and Ni have the same  $2+$  oxidation state in the tetragonal  $\text{ThCr}_2\text{Si}_2$  structure, thus adding one  $d$  electron (hole) contribution by Ni (Fe) substitution for Co in  $\text{BaCo}_2\text{As}_2$  (refs. 20–23), and thereby modifying the electronic structure subtly, but significantly enough to tune in and out of different ground states and correlation types. Utilizing this balance, counter-doping a system to achieve the same nominal  $d$  electron count as  $\text{BaCo}_2\text{As}_2$  can realize a unique route to the same nearly FM system, while disrupting any specific spin correlation in the system.

Here, we utilize this approach to stabilize a novel ground state in the counter-doped nonsuperconducting iron pnictide  $\text{Ba}(\text{Fe}_{1/3}\text{Co}_{1/3}\text{Ni}_{1/3})_2\text{As}_2$ , also nearly FM but with a unique type of spin fluctuation that leads to very strong quasiparticle scattering. We show that NFL behavior is prevalent in the very low-temperature charge transport and thermodynamic properties of  $\text{Ba}(\text{Fe}_{1/3}\text{Co}_{1/3}\text{Ni}_{1/3})_2\text{As}_2$ , with temperature and magnetic energy scale invariance arising from a QC ground state.

## Results

**Non-Fermi liquid magnetotransport.** The hallmark of NFL behavior in  $\text{Ba}(\text{Fe}_{1/3}\text{Co}_{1/3}\text{Ni}_{1/3})_2\text{As}_2$  is clearly observed in the resistivity (Fig. 1a), which exhibits a quasi-linear  $T$  dependence over three orders of magnitude variation, from 20 K down to at least 20 mK at  $B = 0$  T. In this temperature range, we find no discernible anomaly associated with phase transitions down to 20 mK, suggestive of the realization of an anomalous metallic

ground state that persists to the  $T = 0$  limit. Furthermore, this behavior is strongly suppressed with magnetic field, which drives a recovery of Fermi liquid (FL) behavior (i.e.,  $\rho \propto T^2$ ) at low temperatures (Supplementary Note 1).

Note that the unusual resistivity observed in  $\text{Ba}(\text{Fe}_{1/3}\text{Co}_{1/3}\text{Ni}_{1/3})_2\text{As}_2$  cannot be ascribed to either Mooij correlations<sup>24</sup> or quantum interference<sup>25</sup> due to randomness introduced by counter-doping. Given that the Mooij correlations are dominant, increasing randomness enhances the residual resistivity  $\rho_0$ , accompanied by a gradual change in the slope of  $\rho(T)$  at high temperatures, as observed in  $\text{LuRh}_4\text{B}_4$  (ref. 25). However, the overall slope of resistivity in  $\text{Ba}(\text{Fe}_{1/3}\text{Co}_{1/3}\text{Ni}_{1/3})_2\text{As}_2$  is parallel shifted from that in  $\text{BaCo}_2\text{As}_2$  with a sizable increase of residual resistivity by  $\sim 30 \mu\Omega \text{ cm}$ , indicative of the absence of Mooij correlation (Supplementary Note 2). Also, the quasi- $T$ -linear dependence of the resistivity at low temperatures in  $\text{Ba}(\text{Fe}_{1/3}\text{Co}_{1/3}\text{Ni}_{1/3})_2\text{As}_2$  cannot be reproduced by the quantum corrections in conductivity caused by interference that provide the power law  $\sigma \sim T^{p/2}$  (or  $\rho \sim T^{-p/2}$ ), where  $p = 3/2$  (dirty limit), 3 (electron–phonon scattering), or 1 (enhanced electron–electron interaction)<sup>25</sup>. The absence of Mooij correlations and quantum interference allows us to treat scattering sources in charge transport independently. As demonstrated by a smooth change in the temperature slope of resistivity at  $\sim 30$  K (Supplementary Fig. 2), the inelastic scattering dominates over the electron–phonon scattering in the charge transport at low temperatures.

Mimicking the quasi-linear behavior in the temperature dependence of  $\Delta\rho(T) = \rho(T) - \rho(0)$  at 0 T (Fig. 1a inset), the magnetoresistance (MR) at 1.31 K  $\Delta R(B)/R(0)$  varies sublinearly with applied field up to 35 T (Fig. 1b). The quasi-linear  $T$  and  $B$  dependence allow us to introduce a new energy scale involving the scattering rate, the quadrature sum of temperature and magnetic field  $\Gamma(T, B) \equiv \sqrt{(k_B T)^2 + (\eta\mu_B B)^2}$ , where  $\mu_B$  is the Bohr magneton and  $\eta$  is a dimensionless parameter. Here, we treat  $\eta$  as a fitting parameter rather than a value extracted from other measurements or microscopic theoretical calculations. Setting  $\eta = 0.67$ , we find the unusual scaling in the inelastic scattering rate,  $\hbar/\tau = \hbar n e^2 (\rho(T, B) - \rho(0, 0)) / m^*$ , where  $n$  is the carrier density extracted from low-temperature Hall coefficient measured at 0.5 T and  $m^*$  is the effective mass obtained from low-temperature-specific heat measured at 10 T in the present work, as a function of  $\Gamma(T, B)$ , collapsing onto one universal curve as shown in Fig. 1c. This scaling is reminiscent of the observation in QC iron pnictide  $\text{BaFe}_2(\text{As}, \text{P})_2$  (ref. 5). Although  $\text{Ba}(\text{Fe}_{1/3}\text{Co}_{1/3}\text{Ni}_{1/3})_2\text{As}_2$  and  $\text{BaFe}_2(\text{As}, \text{P})_2$  share the similar scaling relation in magnetotransport with each other, we note that while the scaling relation holds in the high  $\Gamma$  region above  $\sim 3$  meV in  $\text{BaFe}_2(\text{As}, \text{P})_2$ , it holds in the low  $\Gamma$  region below  $\sim 2$  meV in  $\text{Ba}(\text{Fe}_{1/3}\text{Co}_{1/3}\text{Ni}_{1/3})_2\text{As}_2$ , and that the extracted value of dimensionless parameter  $\eta$  ( $\eta/\alpha$  in ref. 5) is different from that reported in ref. 5.

The  $\Gamma(T, B)$  scaling can closely be correlated to the Planckian bound of dissipation. Quantum mechanics allows the shortest dissipative time scale  $\tau_p = \hbar/k_B T$ , constrained by the uncertainty principle between dissipative time scale  $\tau$  and energy dissipation  $E \sim k_B T$ ,  $\tau \cdot k_B T \gtrsim \hbar$ . Redefining  $\Gamma(T, B)$  as the dissipation energy scale in magnetic field, we can obtain the universal bound of dissipation,  $\hbar/\tau_p \sim \Gamma(T, B)$ . Our experimental observation in  $\Gamma(T, B)$  scaling for the inelastic scattering gives a linear relation,  $\hbar/\tau = A\Gamma(T, B)$  with  $A = 1.80$ , in good agreement with expected behavior.

Notwithstanding the quasi-two-dimensional layered structure, the NFL magnetotransport is independent of applied field orientations with respect to the FeAs layers. We plot the anisotropy of the MR,  $\Delta\rho(B \parallel c)/\Delta\rho(B \parallel ab)$ , as a function of

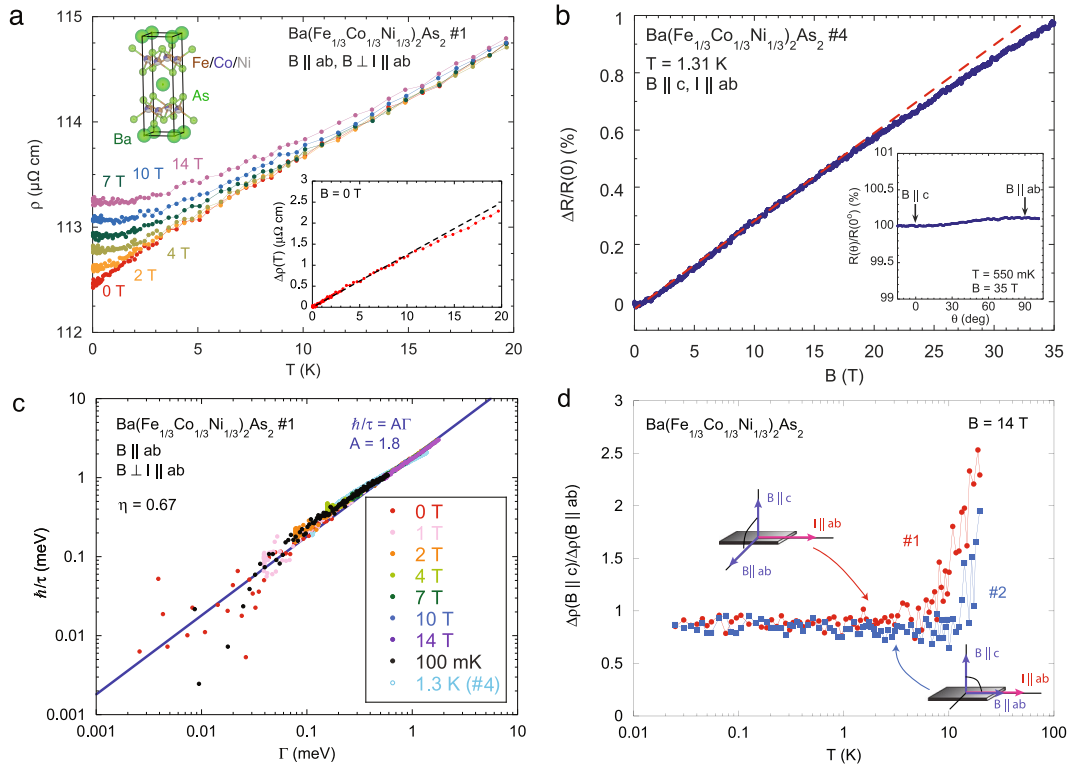


**Fig. 1** Scale invariance in the resistivity of  $\text{Ba}(\text{Fe}_{1/3}\text{Co}_{1/3}\text{Ni}_{1/3})_2\text{As}_2$ . **a** Temperature dependence of resistivity for  $\text{Ba}(\text{Fe}_{1/3}\text{Co}_{1/3}\text{Ni}_{1/3})_2\text{As}_2$  in the configuration of  $B \parallel ab$ ,  $B \perp I \parallel ab$ . Upper inset: crystal structure for  $\text{Ba}(\text{Fe}_{1/3}\text{Co}_{1/3}\text{Ni}_{1/3})_2\text{As}_2$  (ref. 46). Lower inset:  $\Delta\rho(T) = \rho(T) - \rho(0)$  as a function of  $T$  at  $B = 0$  T for  $\text{Ba}(\text{Fe}_{1/3}\text{Co}_{1/3}\text{Ni}_{1/3})_2\text{As}_2$ . A dashed line is a guide to the eye to highlight quasi-linear-in- $T$  dependence of resistivity. **b** Magnetic field dependence of  $\Delta R(B)/R(0) \equiv (R(1.31 \text{ K}, B) - R(1.31 \text{ K}, 0))/R(1.31 \text{ K}, 0)$  at  $T = 1.31$  K. A red dashed line is a guide to the eye to highlight sublinear-in- $B$  behavior of magnetoresistance. Inset: angular dependence of magnetoresistance at  $T = 550$  mK and  $B(\parallel c \perp I) = 35$  T. **c** Inelastic scattering rate  $\hbar/\tau$  as a function of  $\Gamma = \sqrt{(k_B T)^2 + (\eta\mu_B B)^2}$ , with  $\eta = 0.67$ , suggestive of a universal scale invariance in the scattering mechanism in  $\text{Ba}(\text{Fe}_{1/3}\text{Co}_{1/3}\text{Ni}_{1/3})_2\text{As}_2$ . A blue solid line is a linear fit to data using  $\hbar/\tau = A\Gamma$  with  $A = 1.8$ . **d** Temperature dependence of anisotropy of magnetoresistance between  $\Delta\rho(B \parallel c)$  and  $\Delta\rho(B \parallel ab \perp I)$ ; sample #1) and between  $\Delta\rho(B \parallel c)$  and  $\Delta\rho(B \parallel ab \parallel I)$ ; sample #2) at  $B = 14$  T, showing lack of anisotropy in the scattering rate.

temperature in Fig. 1d. The anisotropy between transverse MR in the out-of-plane field ( $B \parallel c$ ,  $I \parallel ab$ ) and transverse MR in the in-plane field ( $B \parallel ab$ ,  $B \perp I \parallel ab$ ) decreases down to unity with decreasing temperatures, suggesting the spatial dimension of the system is three. The isotropy in MR remains even at 35 T, as shown in the angular dependence of MR (Fig. 1 inset). Due to the three dimensionality, we observe similar  $\Gamma(T, B)$  scaling in the resistivity regardless of applied field orientations (Supplementary Note 3). Moreover, the observed positive MR appears not to be driven by the orbital effect due to the Lorentz force, but rather associated with Zeeman energy-tuned scattering, evidenced by the isotropy in the MR between in-plane transverse ( $B \parallel c$ ,  $I \parallel ab$ ) and longitudinal ( $B \parallel I \parallel ab$ ) configurations (Fig. 1d).

**Thermodynamic properties.** In addition to resistivity, magnetic susceptibility  $\chi = M/B$  and electronic heat capacity  $C_e/T$  also exhibit canonical NFL behavior, i.e., diverging temperature dependence associated with QC instabilities<sup>26</sup>. The magnetic susceptibility varies as  $\chi \propto T^{-1/3}$  at low temperatures  $< 8$  K (inset of Fig. 2a), in contrast to the  $T$ -independent Pauli paramagnetic susceptibility  $\chi_p = 2g\mu_B^2 D(E_F)$  (with electron  $g$ -factor and density of states at the Fermi energy  $D(E_F)$ ) observed in FL metals, and observed upon increasing magnetic field to 7 T (Fig. 2a). A similar crossover is also observed in the heat capacity. Obtained from the subtraction of phonon ( $C_{\text{ph}}$ ) and nuclear Schottky contributions ( $C_{\text{Sch}}$ ) from the total heat capacity ( $C_{\text{tot}}$ ), the electronic specific heat coefficient  $C_e/T = (C_{\text{tot}} - C_{\text{ph}} - C_{\text{Sch}})/T$  exhibits power law divergence,  $C_e/T \sim T^{-0.25}$  (Supplementary Note 4), stronger

than logarithmic in the temperature dependence down to  $\sim 150$  mK (Fig. 2b). Diminished with applying field, the NFL behavior observed in zero field completely disappears at applied field of 10 T, indicative of the recovery of FL (Supplementary Note 5). We note that the obtained specific heat coefficient  $\gamma = C_e/T$  at  $B = 0$  T, combined with the magnetic susceptibility  $\chi$ , provides large Wilson ratio  $R_W = \pi^2 k_B^2 \chi / 3\mu_B^2 \gamma = 3.2$  at  $T = 1.8$  K, suggestive of the presence of magnetic instabilities similar to  $\text{BaCo}_2\text{As}_2$ .

The observation of FL recovery with magnetic field corroborates the presence of a new energy scale  $k_B T^*$ , distinctive of crossover between the QC ( $k_B T \gg g\mu_B B$ ) and FL ( $k_B T \ll g\mu_B B$ ) regimes. Intriguingly, this new energy scale allows a single scaling function of  $T/B$  in the magnetization, written by,

$$-\frac{dM}{dT} = B^{-\frac{1}{3}} f_M\left(\frac{T}{B}\right), \quad (1)$$

as shown in Fig. 2c. This scaling relation indeed reveals the underlying free energy given by a universal function of  $T/B$ ,

$$F(T, B) = B^{(d+z)/y_b} f_F\left(\frac{T}{B^{z/y_b}}\right), \quad (2)$$

where  $d$  is the spatial dimensionality,  $z$  is the dynamic exponent, and  $y_b$  is the scaling exponent related to the tuning parameter  $B$  (refs. 27–30). Here,  $f_F(x)$  is a universal function of  $x$ . Hence, the magnetization can be derived from the derivative of the free

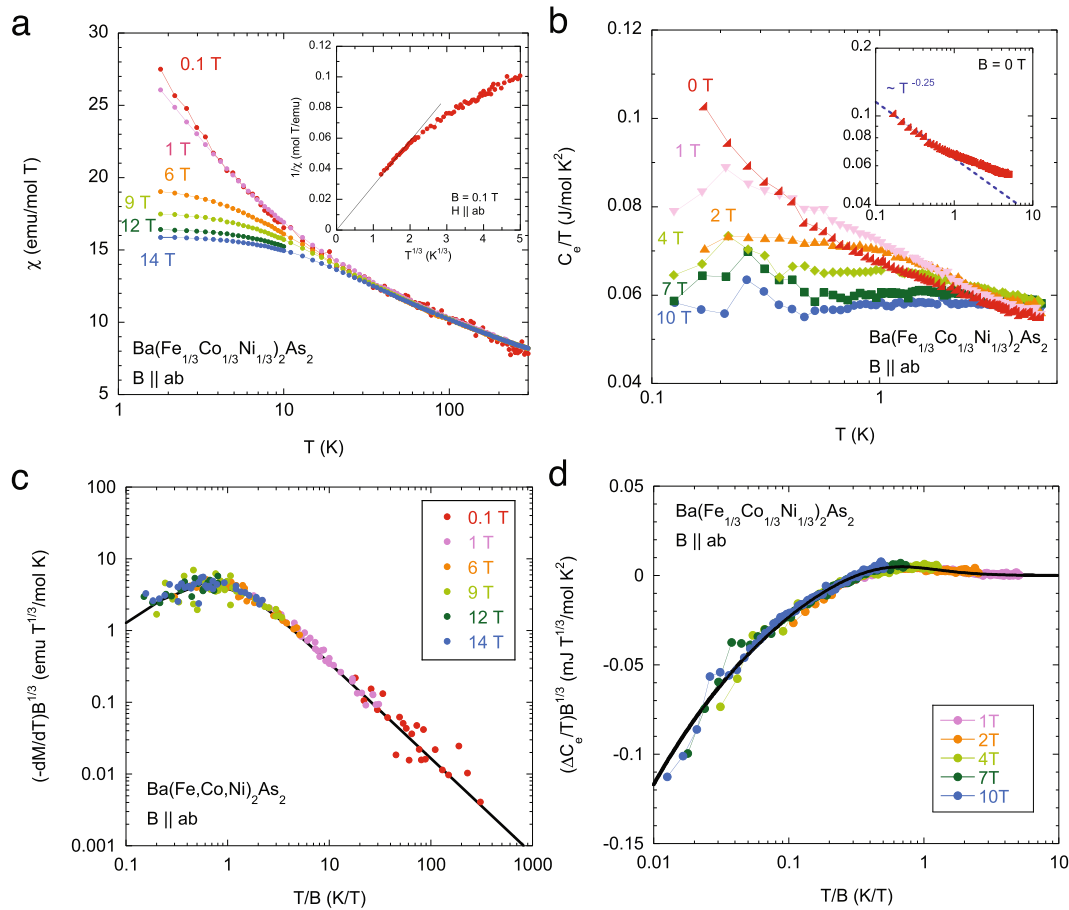


**Fig. 2 Non-Fermi liquid to Fermi liquid crossover and scale invariance in thermodynamic quantities.** **a** Temperature dependence of magnetic susceptibility for  $\text{Ba}(\text{Fe}_{1/3}\text{Co}_{1/3}\text{Ni}_{1/3})_2\text{As}_2$  ( $B \parallel ab$ ). Inset:  $1/\chi$  as a function of  $T^{1/3}$  at low temperatures. **b** Electronic specific heat  $C_e/T = (C_{\text{tot}} - C_{\text{sch}} - C_{\text{ph}})/T$  for  $\text{Ba}(\text{Fe}_{1/3}\text{Co}_{1/3}\text{Ni}_{1/3})_2\text{As}_2$  under several fields parallel to  $ab$ -plane. Inset: log-log plot for  $C_e/T$  vs  $T$  for  $B = 0$  T. The dashed line emphasizes the  $T^{-0.25}$ -power law behavior observed  $<1$  K. **c** Temperature-magnetic field scale invariance in magnetization and **d** specific heat. The measured magnetization and specific heat collapse onto universal scaling curves in the forms of  $-dM/dT = B^{-1/3}f_M(T/B)$  and  $\Delta C_e/T = B^{-1/3}g_C(T/B)$ , respectively, indicating the presence of the underlying free energy given by a universal function of  $T/B$  and the existence of the quantum critical point located at  $T = 0$  and  $B = 0$ . Black lines represent scaling functions  $f_M(T/B)$  for magnetization and  $g_C(T/B)$  for specific heat derived from the underlying free energy, described in the main text.

energy,

$$-\frac{dM}{dT} = -\frac{d}{dT} \left( \frac{dF}{dB} \right) = B^{d/y_b-1} f_M \left( \frac{T}{B^{z/y_b}} \right). \quad (3)$$

Directly comparing this with the observed QC scaling relation in Fig. 2c, we can extract the critical exponents in the free energy, namely,  $z/y_b = 1$  and  $d/y_b - 1 = -1/3$ , yielding  $z = y_b$  and  $d/z = 2/3$ . These values of the critical exponents describe the specific heat by using the same free energy,

$$\frac{C_e(B, T)}{T} = -\frac{\partial^2 F}{\partial T^2} = B^{\frac{d-z}{y_b}} f_C \left( \frac{T}{B^{z/y_b}} \right). \quad (4)$$

Rewriting the free energy,  $F(T, B) = B^{\frac{d+z}{y_b}} f(T/B^{z/y_b}) = T^{\frac{d+z}{z}} \tilde{f}(B/T^{y_b/z})$ , we find

$$\frac{\Delta C_e(T, B)}{T} = \frac{C_e(T, B)}{T} - \frac{C_e(T, 0)}{T} = B^{-\frac{1}{3}} g_C \left( \frac{T}{B} \right), \quad (5)$$

where  $g_C(x)$  is field-dependent part of  $f_C(x)$  (Supplementary Notes 6 and 7). As demonstrated in Fig. 2d, this expression illustrates scale invariance in the specific heat that persists over nearly three orders of magnitude in the scaling variable  $T/B$ .

**Hall resistivity and electronic structure.** The  $T/B$  scaling in thermodynamics clearly discloses the presence of the QCP located exactly at zero field and absolute zero, similar to the layered QC metals  $\text{YbAlB}_4$  (ref. 31) and  $\text{YFe}_2\text{Al}_{10}$  (ref. 32). More notably, the multiband nature in iron pnictides affixes the uniqueness of quantum criticality for  $\text{Ba}(\text{Fe}_{1/3}\text{Co}_{1/3}\text{Ni}_{1/3})_2\text{As}_2$ . Dominated by electron-like carriers, the Hall resistivity  $\rho_{yx}$  is negative and perfectly linear in field at high temperatures ( $T = 20$  K), as shown in Fig. 3a. Upon cooling,  $\rho_{yx}$  develops a nonlinearity with negative curvature. More prominent  $<1$  K, the nonlinear Hall resistivity switches its sign at low fields  $<2$  T. The sign change is more readily observed in the temperature dependence of Hall coefficient  $R_H$  defined by  $\rho_{yx}/B$  at low- $T$  and low- $H$  region (Fig. 3b), implying that hole-like carriers dominate the transport in the vicinity of the QCP. The radial shape of the dominant carrier crossover in the field-temperature phase diagram confirms the absence of an intrinsic energy scale in  $R_H$  (Fig. 3c), or in other words, the presence of scale invariance in the Hall effect tuned by temperature and magnetic field. Similar to the resistivity,  $R_H$  obeys  $\Gamma(T, B)$  scaling (Fig. 3d), consolidating the existence of scale invariance near the QCP in this system beyond any doubt.

Angle-resolved photoemission measurements identify a unique electronic structure and confirm the anomalous scattering rate

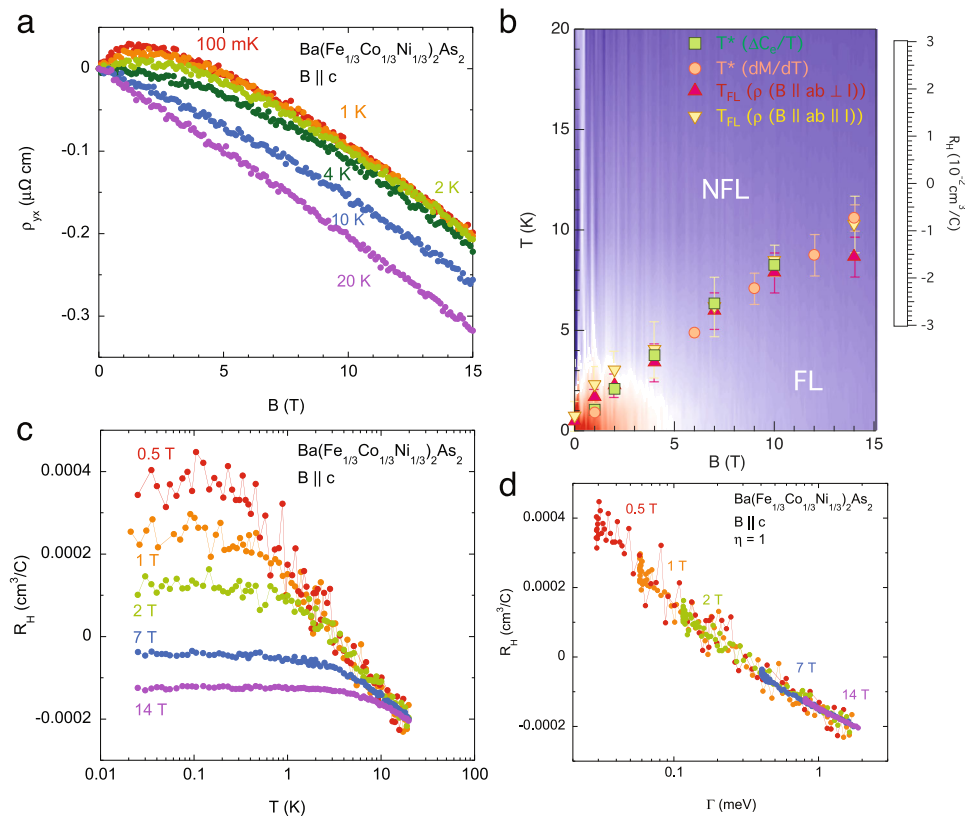


**Fig. 3 Sign change due to dominant hole-like carriers near the quantum critical point and scale invariance in Hall effect.** **a** Hall resistivity  $\rho_{yx}$  as a function of  $B$ . At high temperatures,  $\rho_{yx}$  is negative and linear in field. Upon cooling temperatures,  $\rho_{yx}$  becomes nonlinear and its sign switches to positive at low fields  $< 2$  T. **b** Temperature dependence of Hall coefficient  $R_H$  defined by  $\rho_{yx}/B$ . **c**  $T - B$  phase diagram with color plot of  $R_H$ . Crossover temperatures  $T^*$  obtained from the quantum scaling in  $dM/dT$  and  $\Delta C_v/T$  and  $T_{FL}$  from the  $T^2$ -fit are also plotted in the phase diagram. The error bars of  $T^*$  represent the standard deviation, and the error bars of  $T_{FL}$  are estimated by changing the fitting range. **d**  $R_H$  as a function of  $\Gamma(T, B) \equiv \sqrt{(k_B T)^2 + (\eta \mu_B B)^2}$  with  $\eta = 1$ . All the data collapse onto one universal curve, suggesting unusual scaling between temperature and applied field similar to that found in the longitudinal resistivity.

correlated with Planckian dissipation. Unlike heavily electron-doped  $\text{BaCo}_2\text{As}_2$ , the electronic structure for  $\text{Ba}(\text{Fe}_{1/3}\text{Co}_{1/3}\text{Ni}_{1/3})_2\text{As}_2$  consists of a large hole-like pocket and a cross-shaped electron-like Fermi surface around the  $\Gamma$  point, together with oval and elongated electron pockets around the  $M$  points, exhibited by the Fermi surface map (Fig. 4a), the band dispersion along  $k_x = 0$  direction (Fig. 4b) at 30 K, and a schematic illustration (Fig. 4a, inset). The elongated electron pockets are very shallow, and the chemical potential is located close to the bottom of the shallow bands. Dominating transport at low temperatures and fields, the large hole-like pocket is identified as the one responsible for QC behavior. Amazingly, the scattering rate (obtained from the dispersion of the hole-like bands at 1 K) varies linearly with the kinetic energy up to 100 meV, consistent with Planckian dissipation as observed in the resistivity (Fig. 4c, d).

## Discussion

While our primary observations of the scale invariance in the thermodynamics are consistent with quantum criticality overall, they indicate a highly unusual critical behavior in  $\text{Ba}(\text{Fe}_{1/3}\text{Co}_{1/3}\text{Ni}_{1/3})_2\text{As}_2$ . While sharing an enhancement of the Wilson ratio with  $\text{BaCo}_2\text{As}_2$  indicative of a FM instability, the critical behavior in  $\text{Ba}(\text{Fe}_{1/3}\text{Co}_{1/3}\text{Ni}_{1/3})_2\text{As}_2$  is not described by any known theoretical predictions. Assuming spacial dimensionality of three ( $d=3$ ) based on the observed isotropic response in MR and magnetization (Supplementary Note 3), the observed critical exponents of  $d/z = 2/3$  and  $z = \gamma_b$  yield  $z = \gamma_b = 4.5$ .

The extracted dynamical exponents from our measurements do not match the predictions for either mean-field Hertz–Moriya–Millis theory for  $d=3$  (which predict  $z = 3$  for clean FM and  $z = 4$  for

dirty FM quantum criticality with  $\nu = 1/2$ )<sup>27–29</sup>, or predictions for clean FM beyond mean field, which predict the appearance of a weak first-order transition, with  $z = 3$  and  $\nu = 1/4$  for  $d = 3$  and quantum wing critical points with the same critical exponents, as the mean-field theory<sup>33–37</sup>. QC behavior in disordered 3d FM has been well explained by the Belitz–Kirkpatrick–Vojta theory, predicting critical exponents  $\nu = 1$  and  $z = 3$  for the asymptotic limit, and  $\nu = 0.25$  and  $z = 6$  for the preasymptotic limit<sup>37, 38</sup>, neither of which is in agreement with our observation. Experimentally, previously measured exponents in QC materials, such as  $\text{YbNi}_4(\text{P}_{1-x}\text{As}_x)_2$  (FM QCP,  $\nu z \sim 5$ )<sup>39</sup>,  $\text{CeCu}_{6-x}\text{Au}_x$  (AFM QCP,  $d/z = 1/4$ ,  $\nu z = 1$ )<sup>40</sup>,  $\beta\text{-YbAlB}_4$  (mixed-valence metal,  $d/z = 1/2$ ,  $\nu z = 1$ )<sup>31</sup>,  $\text{YFe}_2\text{Al}_{10}$  (layered QC metal,  $d/z = 1$ ,  $\nu z = 0.59$ )<sup>32</sup>, and  $\text{Sr}_{0.3}\text{Ca}_{0.7}\text{RuO}_3$  (disordered FM QCP,  $z = 1.76$ )<sup>41</sup> are also incompatible with the measured dynamical exponent.

The high residual resistivity observed in  $\text{Ba}(\text{Fe}_{1/3}\text{Co}_{1/3}\text{Ni}_{1/3})_2\text{As}_2$  evokes the possible realization of quantum Griffiths phase, where the QC behavior is dominated by FM rare regions. The quantum Griffiths model predicts power law singularities in the magnetic susceptibility ( $\chi \sim T^{\lambda-1}$ ), specific heat ( $C/T \sim T^{\lambda-1}$ ), and magnetization ( $M \sim B^\lambda$ ), determined by the nonuniversal Griffiths exponent  $\lambda$  that takes 0 at the QCP, and increases with distance from criticality<sup>42</sup>. In the present system, however,  $\lambda = 2/3$  extracted from the magnetic susceptibility ( $\chi \sim T^{-1/3}$ ; Fig. 1a inset) disagrees with  $\lambda = 0.75$  obtained from the specific heat ( $C/T \sim T^{-0.25}$ ; Fig. 2b inset), irreconcilable with the quantum Griffiths model. Besides, the critical exponents in  $\text{Ba}(\text{Fe}_{1/3}\text{Co}_{1/3}\text{Ni}_{1/3})_2\text{As}_2$  do not agree with those obtained experimentally in other quantum Griffith systems<sup>37</sup>. For instance, disordered weak ferromagnet  $\text{Ni}_{1-x}\text{V}_x$  show critical

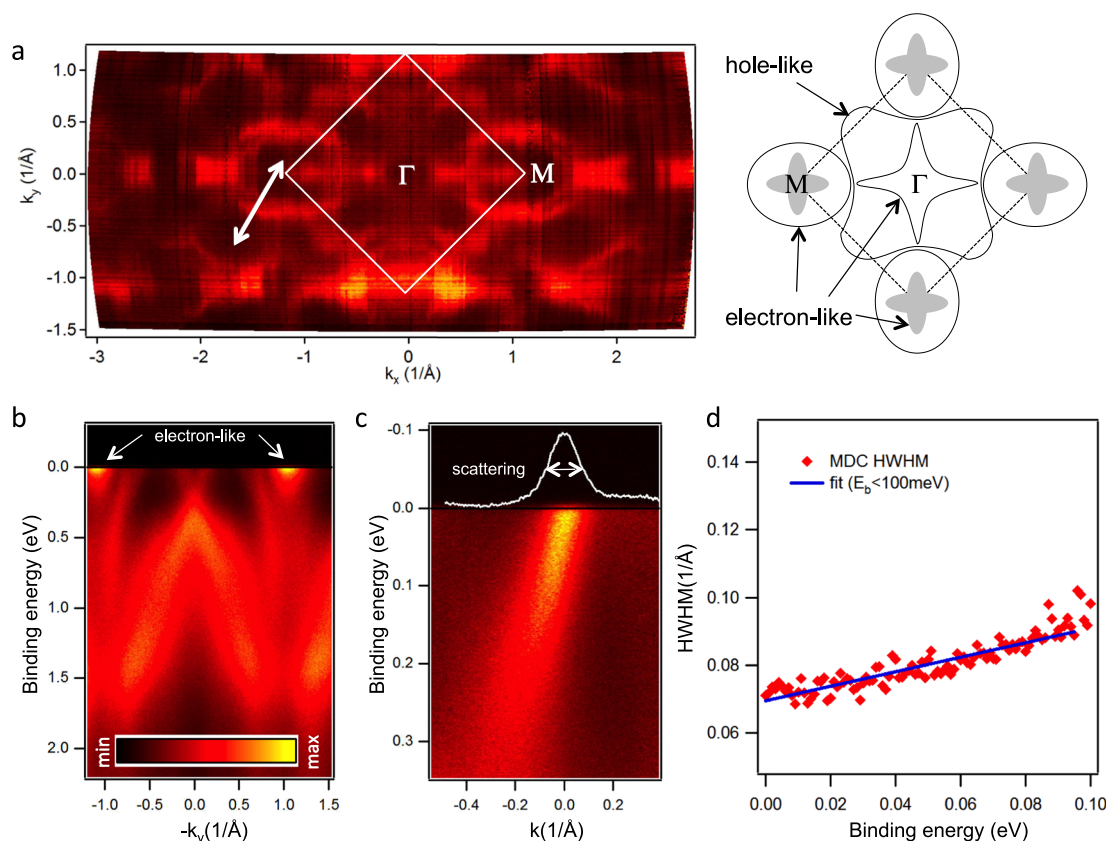


**Fig. 4** Fermi surfaces and anomalous scattering rates in  $\text{Ba}(\text{Fe}_{1/3}\text{Co}_{1/3}\text{Ni}_{1/3})_2\text{As}_2$ . **a** Angle-resolved photoemission study of Fermi surface map for  $\text{Ba}(\text{Fe}_{1/3}\text{Co}_{1/3}\text{Ni}_{1/3})_2\text{As}_2$ , measured at 30 K. White lines denote the Brillouin zone (BZ) boundary, and white arrow corresponds to the cut shown in **c**. The inset depicts a schematic Fermi surface corresponding to the experimentally observed data, with shallow elongated electron pockets shown in gray. **b** Energy cut along the  $k_x = 0$  direction, highlighting the elongated shallow electron-like pockets observed near the BZ corners. **c** Energy dispersion of hole-like pocket measured at 1 K near the BZ boundary along the cut indicated by white arrow in **a**, where sharp crossings of the Fermi level are found. The momentum axis originates at the crossing point. The white spectrum is the momentum distribution curve (MDC) at the Fermi level, with indicated width a representative measure of the scattering rate. **d** Scattering rate energy dependence obtained from the half width at half maximum (HWHM) of energy dispersion in panel **c**, with linear fit up to 100 meV.

behavior dominated by quantum Griffiths singularities,  $\chi \sim T^{\lambda-1}$  and  $M \sim B^\lambda$ , over a wide range of vanadium concentration<sup>43, 44</sup>. On the other hand, in  $\text{Ba}(\text{Fe}_{1/3}\text{Co}_{1/3}\text{Ni}_{1/3})_2\text{As}_2$ ,  $\lambda = 2/3$  derived from the magnetic susceptibility contradicts  $\lambda$  obtained from magnetization  $M \sim B^{0.75}$  (Supplementary Fig. 5), in conflict with the quantum Griffiths phase.

Highly unusual dynamical critical behavior in this material cannot be simply explained by existing FM QCP theories, but instead, it can be attributed to substitutional alloying by counter-doping. Indeed, the anomalous behavior observed in  $\text{Ba}(\text{Fe}_{1/3}\text{Co}_{1/3}\text{Ni}_{1/3})_2\text{As}_2$  is more prominent than that observed in both of the end members of the  $3d^7$  configuration line, namely,  $\text{BaCo}_2\text{As}_2$  and  $\text{Ba}(\text{Fe,Ni})_2\text{As}_2$  (Supplementary Notes 8 and 9), signifying that the specific 1/3 equal ratios of Fe:Co:Ni in  $\text{BaCo}_2\text{As}_2$  are indeed important to stabilizing a unique QC ground state. In fact, as shown in Fig. 5, the observed NFL scattering behavior in  $\text{Ba}(\text{Fe}_{1/3}\text{Co}_{1/3}\text{Ni}_{1/3})_2\text{As}_2$  is completely robust against pressure and even replacement of Ba for Sr (i.e., in  $\text{Sr}(\text{Fe}_{1/3}\text{Co}_{1/3}\text{Ni}_{1/3})_2\text{As}_2$ ), implying either an electronic structure modification beyond  $d$  electron tuning, or a significant role for transition metal site dilution. In fact, while generally obscuring the critical behavior, high randomness due to substitution indeed plays an important role in some QC materials, such as medium entropy alloys<sup>38, 45</sup>, in which similar NFL behavior has been realized<sup>38, 45</sup>. Together with the pressure insensitivity of the  $T$ -linear scattering in  $\text{Ba}(\text{Fe}_{1/3}\text{Co}_{1/3}\text{Ni}_{1/3})_2\text{As}_2$ , our experimental observations of scale invariance in this system indicates that

substitutional alloying is a key ingredient to tune the quantum criticality that may provide the key to understanding the lack of superconductivity driven by QC fluctuations.

## Methods

**Sample preparation.** The single crystals of  $\text{Ba}(\text{Fe}_{1/3}\text{Co}_{1/3}\text{Ni}_{1/3})_2\text{As}_2$  were grown by TMAs (TM = Fe, Co, and Ni) self-flux method with the molar ratios of 3:4:4:4 = Ba:FeAs:CoAs:NiAs. Resulting crystals were cleaved out of the flux. The typical crystal size is  $5 \times 5 \times 0.1 \text{ mm}^3$ .

**Magnetotransport measurements.** Magnetotransport measurements up to 15 T were conducted in a  $^3\text{He}$ - $^4\text{He}$  dilution refrigerator, and high magnetic field transport measurements up to 35 T were performed at the National High Magnetic Field Laboratory in Tallahassee.

**Heat capacity measurements.** Heat capacity was measured using the thermal relaxation method in a  $^3\text{He}$ - $^4\text{He}$  dilution refrigerator. A  $\text{RuO}_2$  thermometer on the calorimeter was calibrated in magnetic fields up to 15 T.

**Magnetic susceptibility measurements.** Magnetic susceptibility was measured using the vibrating sample magnetometer option in a 14 T Quantum Design DynaCool Physical Properties Measurement System and a 7 T SQUID Magnetic Properties Measurement System.

**Pressure measurements.** A nonmagnetic piston-cylinder pressure cell was used for transport measurements under pressure up to 1.99 GPa, using a 1:1 ratio of  $n$ -pentane to 1-methyl-3-butanol as the pressure medium, and superconducting temperature of lead as pressure gauge at base temperature. All transport measurements were performed on the same  $\text{Ba}(\text{Fe}_{1/3}\text{Co}_{1/3}\text{Ni}_{1/3})_2\text{As}_2$  crystal with 200

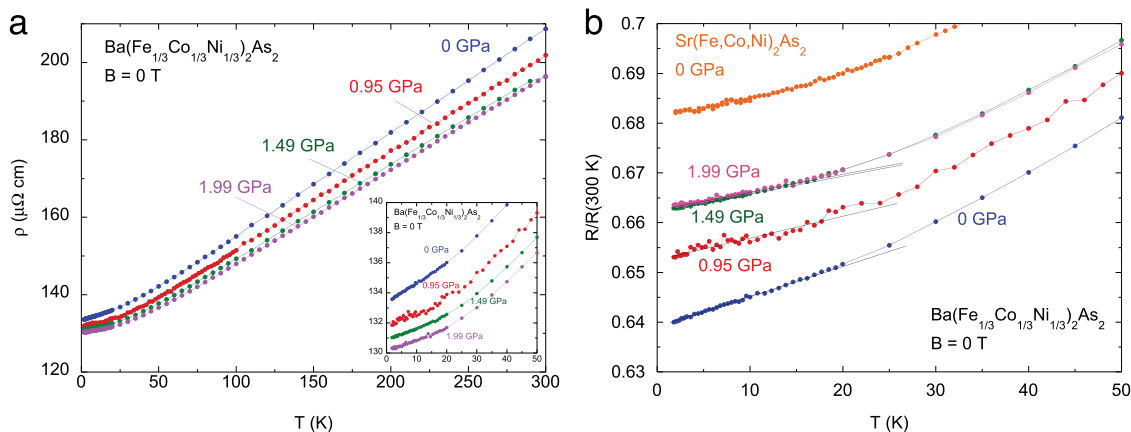


**Fig. 5 Robust non-Fermi liquid behavior against pressure.** **a** Overall temperature dependence of resistivity for  $\text{Ba}(\text{Fe}_{1/3}\text{Co}_{1/3}\text{Ni}_{1/3})_2\text{As}_2$  under applied pressure. The linear- $T$  resistivity  $< 20$  K is robust against applying pressure up to 1.99 GPa as shown in the inset. **b** Normalized resistance  $R/R(300\text{ K})$  vs  $T$  under pressure. On applying pressure,  $R/R(300\text{ K})$  for  $\text{Ba}(\text{Fe}_{1/3}\text{Co}_{1/3}\text{Ni}_{1/3})_2\text{As}_2$  increases, approaching that for  $\text{Sr}(\text{Fe}_{1/3}\text{Co}_{1/3}\text{Ni}_{1/3})_2\text{As}_2$  with smaller lattice constants than  $\text{Ba}(\text{Fe}_{1/3}\text{Co}_{1/3}\text{Ni}_{1/3})_2\text{As}_2$  (Supplementary Notes 10 and 11, and Supplementary Table 1), indicative of robustness of linear- $T$  behavior in the resistivity against pressure.

$\mu\text{m}$  thickness, using four point contacts made with silver epoxy. The pressure and temperature dependence of the resistivity were measured during warming process in a Quantum Design Physical Properties Measurement System. Mention of commercial equipment does not imply endorsement by NIST.

**Angle-resolved photoemission spectroscopy.** Angle-resolved photoemission spectroscopy for  $\text{Ba}(\text{Fe}_{1/3}\text{Co}_{1/3}\text{Ni}_{1/3})_2\text{As}_2$  was performed using the  $1^3$ -ARPES end station of the UE112-PGM2b beam-line at BESSY II (Helmholtz Zentrum Berlin) synchrotron radiation center.

#### Data availability

All data presented in this manuscript are available from the corresponding author upon reasonable request.

Received: 25 June 2020; Accepted: 11 September 2020;

Published online: 15 October 2020

#### References

- Paglione, J. & Greene, R. L. High-temperature superconductivity in iron-based materials. *Nat. Phys.* **6**, 645–658 (2010).
- Shibauchi, T., Carrington, A. & Matsuda, Y. A quantum critical point lying beneath the superconducting dome in iron pnictides. *Annu. Rev. Condens. Matter Phys.* **5**, 113–135 (2014).
- Mazin, I. L., Singh, D. J., Johannes, M. D. & Du, M. H. Unconventional superconductivity with a sign reversal in the order parameter of  $\text{LaFeAsO}_{1-x}\text{F}_x$ . *Phys. Rev. Lett.* **101**, 057003 (2008).
- Kuroki, K., Usui, H., Onari, S., Arita, R. & Aoki, H. Pnictogen height as a possible switch between high- $T_c$  nodeless and low- $T_c$  nodal pairings in the iron-based superconductors. *Phys. Rev. B* **79**, 224511 (2009).
- Hayes, I. M. et al. Scaling between magnetic field and temperature in the high-temperature superconductor  $\text{BaFe}_2(\text{As}_{1-x}\text{P}_x)_2$ . *Nat. Phys.* **12**, 916–919 (2016).
- Giraldo-Gallo, P. et al. Scale-invariant magnetoresistance in a cuprate superconductor. *Science* **361**, 479–481 (2018).
- Legros, A. et al. Universal  $T$ -linear resistivity and planckian dissipation in overdoped cuprates. *Nat. Phys.* **15**, 142–147 (2019).
- Guo, H., Gu, Y. & Sachdev, S. Linear in temperature resistivity in the limit of zero temperature from the time reparameterization soft mode. *Ann. Phys.* **418**, 168202 (2020).
- Chu, J.-H. et al. In-plane resistivity anisotropy in an underdoped iron arsenide superconductor. *Science* **329**, 824–826 (2010).
- Yi, M. et al. Symmetry-breaking orbital anisotropy observed for detwinned  $\text{Ba}(\text{Fe}_{1-x}\text{Co}_x)_2\text{As}_2$  above the spin density wave transition. *Proc. Natl Acad. Sci. USA* **108**, 6878–6883 (2011).
- Nakajima, M. et al. Unprecedented anisotropic metallic state in undoped iron arsenide  $\text{BaFe}_2\text{As}_2$  revealed by optical spectroscopy. *Proc. Natl Acad. Sci. USA* **108**, 12238–12242 (2011).
- Chu, J.-H., Kuo, H.-H., Analytis, J. G. & Fisher, I. R. Divergent nematic susceptibility in an iron arsenide superconductor. *Science* **337**, 710–712 (2012).
- Yanagi, H. et al. Itinerant ferromagnetism in the layered crystals  $\text{LaCoOX}$  ( $X=\text{P,As}$ ). *Phys. Rev. B* **77**, 224431 (2008).
- Anand, V. K. et al. Crystallography and physical properties of  $\text{BaCo}_2\text{As}_2$ ,  $\text{Ba}_{0.94}\text{K}_{0.06}\text{Co}_2\text{As}_2$ , and  $\text{Ba}_{0.78}\text{K}_{0.22}\text{Co}_2\text{As}_2$ . *Phys. Rev. B* **90**, 064517 (2014).
- Wiecki, P. et al. Competing magnetic fluctuations in iron pnictide superconductors: role of ferromagnetic spin correlations revealed by NMR. *Phys. Rev. Lett.* **115**, 137001 (2015).
- Wiecki, P., Ogloblichev, V., Pandey, A., Johnston, D. C. & Furukawa, Y. Coexistence of antiferromagnetic and ferromagnetic spin correlations in  $\text{SrCo}_2\text{As}_2$  revealed by  $^{59}\text{Co}$  and  $^{75}\text{As}$  NMR. *Phys. Rev. B* **91**, 220406 (2015).
- Sefat, A. S. et al. Renormalized behavior and proximity of  $\text{BaCo}_2\text{As}_2$  to a magnetic quantum critical point. *Phys. Rev. B* **79**, 024512 (2009).
- Sefat, A. S. et al. Structure and anisotropic properties of  $\text{BaFe}_2-x\text{Ni}_x\text{As}_2$  ( $x=0, 1$ , and 2) single crystals. *Phys. Rev. B* **79**, 094508 (2009).
- Eckberg, C. et al. Evolution of structure and superconductivity in  $\text{Ba}(\text{Ni}_{1-x}\text{Co}_x)_2\text{As}_2$ . *Phys. Rev. B* **97**, 224505 (2018).
- Ni, N. et al. Phase diagrams of  $\text{Ba}(\text{Fe}_{1-x}\text{M}_x)_2\text{As}_2$  single crystals ( $\text{M}=\text{Rh}$  and  $\text{Pd}$ ). *Phys. Rev. B* **80**, 024511 (2009).
- Canfield, P. C., Bud'ko, S. L., Ni, N., Yan, J. Q. & Kracher, A. Decoupling of the superconducting and magnetic/structural phase transitions in electron-doped  $\text{BaFe}_2\text{As}_2$ . *Phys. Rev. B* **80**, 060501 (2009).
- Liu, C. et al. Evidence for a Lifshitz transition in electron-doped iron arsenic superconductors at the onset of superconductivity. *Nat. Phys.* **6**, 419–423 (2010).
- Neupane, M. et al. Electron-hole asymmetry in the superconductivity of doped  $\text{BaFe}_2\text{As}_2$  seen via the rigid chemical-potential shift in photoemission. *Phys. Rev. B* **83**, 094522 (2011).
- Ciuchi, S., Di Sante, D., Dobrosavljević, V. & Fratini, S. The origin of moiré correlations in disordered metals. *npj Quantum Mater.* **3**, 44 (2018).
- Lee, P. A. & Ramakrishnan, T. V. Disordered electronic systems. *Rev. Mod. Phys.* **57**, 287–337 (1985).
- Stewart, G. Non-fermi-liquid behavior in d- and f-electron metals. *Rev. Mod. Phys.* **73**, 797 (2001).
- Hertz, J. A. Quantum critical phenomena. *Phys. Rev. B* **14**, 1165 (1976).
- Moriya, T. *Spin Fluctuations in Itinerant Electron Magnetism* (Springer, Berlin, Heidelberg, Germany, 1985).
- Millis, A. J. Effect of a nonzero temperature on quantum critical points in itinerant fermion systems. *Phys. Rev. B* **48**, 7183–7196 (1993).
- Sachdev, S. *Quantum Phase Transitions* (Cambridge University Press, Cambridge, UK, 1999).
- Matsumoto, Y. et al. Quantum criticality without tuning in the mixed valence compound  $\beta\text{-YbAlB}_4$ . *Science* **331**, 316–319 (2011).
- Wu, L. S., Kim, M. S., Park, K., Tselik, A. M. & Aronson, M. C. Quantum critical fluctuations in layered  $\text{YFe}_2\text{Al}_{10}$ . *Proc. Natl Acad. Sci. USA* **111**, 14088–14093 (2014).
- Belitz, D., Kirkpatrick, T. R. & Vojta, T. Nonanalytic behavior of the spin susceptibility in clean fermi systems. *Phys. Rev. B* **55**, 9452–9462 (1997).

34. Rech, J., Pépin, C. & Chubukov, A. V. Quantum critical behavior in itinerant electron systems: Eliashberg theory and instability of a ferromagnetic quantum critical point. *Phys. Rev. B* **74**, 195126 (2006).
35. Conduit, G. J., Green, A. G. & Simons, B. D. Inhomogeneous phase formation on the border of itinerant ferromagnetism. *Phys. Rev. Lett.* **103**, 207201 (2009).
36. Kirkpatrick, T. R. & Belitz, D. Exponent relations at quantum phase transitions with applications to metallic quantum ferromagnets. *Phys. Rev. B* **91**, 214407 (2015).
37. Brando, M., Belitz, D., Grosche, F. M. & Kirkpatrick, T. R. Metallic quantum ferromagnets. *Rev. Mod. Phys.* **88**, 025006 (2016).
38. Sales, B. C. et al. Quantum critical behavior in the asymptotic limit of high disorder in the medium entropy alloy NiCoCr<sub>0.8</sub>. *npj Quantum Mater.* **2**, 33 (2017).
39. Steppke, A. et al. Ferromagnetic quantum critical point in the heavy-fermion metal YbNi<sub>4</sub>(P<sub>1-x</sub>As<sub>x</sub>)<sub>2</sub>. *Science* **339**, 933–936 (2013).
40. Schroeder, A. et al. Onset of antiferromagnetism in heavy-fermion metals. *Nature* **407**, 351 (2000).
41. Huang, C. L. et al. Anomalous quantum criticality in an itinerant ferromagnet. *Nat. Commun.* **6**, 8188 (2015).
42. Vojta, T. Quantum Griffiths effects and smeared phase transitions in metals: theory and experiment. *J. Low. Temp. Phys.* **161**, 299–323 (2010).
43. Ubaid-Kassis, S., Vojta, T. & Schroeder, A. Quantum Griffiths phase in the weak itinerant ferromagnetic alloy Ni<sub>1-x</sub>V<sub>x</sub>. *Phys. Rev. Lett.* **104**, 066402 (2010).
44. Wang, R. et al. Quantum Griffiths phase inside the ferromagnetic phase of Ni<sub>1-x</sub>V<sub>x</sub>. *Phys. Rev. Lett.* **118**, 267202 (2017).
45. Sales, B. C. et al. Quantum critical behavior in a concentrated ternary solid solution. *Sci. Rep.* **6**, 26179 (2016).
46. Momma, K. & Izumi, F. VESTA3 for three-dimensional visualization of crystal, volumetric and morphology data. *J. Appl. Crystallogr.* **44**, 1272–1276 (2011).

## Acknowledgements

Experimental research was supported by the National Science Foundation Division of Materials Research Award No. DMR-1610349, and materials development supported by the Gordon and Betty Moore Foundation's EPiQS Initiative through grant no. GBMF9071. A portion of this work was performed at the National High Magnetic Field Laboratory, which is supported by National Science Foundation Cooperative Agreement No. DMR-1644779 and the State of Florida. Pressure measurements were supported by NIST.

## Author contributions

Y.N., T.M., K.K., A.H., and R.W. performed the low-temperature transport and heat capacity measurements, and analyzed the data. C.E. and S.R.S. grew and characterized single crystals. I.L. and N.B. conducted the pressure measurements, and D.C., Y.S.E., and D.G. performed transport measurements at high magnetic fields. Z.L. and S.V.B. measured the angle-resolved photoemission spectroscopy, and L.W. performed the theoretical support. P.Y.Z. performed the single-crystal x-ray diffraction. Y.N. and J.P. conceived and designed the experiments, and all authors contributed to the editing of the manuscript.

## Competing interests

The authors declare no competing interests.

## Additional information

**Supplementary information** is available for this paper at <https://doi.org/10.1038/s42005-020-00448-5>.

**Correspondence** and requests for materials should be addressed to Y.N. or J.P.

**Reprints and permission information** is available at <http://www.nature.com/reprints>

**Publisher's note** Springer Nature remains neutral with regard to jurisdictional claims in published maps and institutional affiliations.



**Open Access** This article is licensed under a Creative Commons Attribution 4.0 International License, which permits use, sharing, adaptation, distribution and reproduction in any medium or format, as long as you give appropriate credit to the original author(s) and the source, provide a link to the Creative Commons license, and indicate if changes were made. The images or other third party material in this article are included in the article's Creative Commons license, unless indicated otherwise in a credit line to the material. If material is not included in the article's Creative Commons license and your intended use is not permitted by statutory regulation or exceeds the permitted use, you will need to obtain permission directly from the copyright holder. To view a copy of this license, visit <http://creativecommons.org/licenses/by/4.0/>.

© The Author(s) 2020